On the Nature of the Interaction Between Structures and Proof-Mass Actuators

David C. Zimmerman*
University of Florida, Gainesville, Florida
and
Daniel J. Inman†
Brown University, Providence, Rhode Island

This paper presents an analysis of the interaction between a structure, an actuator used to control the vibration of the structure, and the control law to be implemented by the actuator. The control hardware used is a proof-mass actuator with experimentally verified dynamics capable of being used in a space structure configuration. A local rate-feedback control law is used. The control of two different structures is presented. The first structure is a cantilevered beam constructed of a quasi-isotropic composite material that is controlled by a single actuator forming the experimental component of the investigation. The second structure is a finite-element model of a truss system controlled by a single actuator. Models of both structures predict the presence of potential instabilities in system performance if proper consideration is not given to interactions between the control law, the structure, and the actuator.

I. Introduction

THE control of large flexible space structures by a small number of control devices acting at a few points along the structure has sparked intensive research over the last ten years.[1-3] A majority of the work in this area has neglected the effects of actuator dynamics in modeling the closed-loop system. Recently, concern has developed over the effects of actuator dynamics in the design of control laws for flexible structures.[4-6] The emphasis of this paper is to examine the effects that both actuator dynamics and control forces have on the performance of the actuator/structure system. Both experimental and numerical results are presented.

The control device used in this work is a proof-mass actuator (PMA) developed for the Structural Dynamics Branch of the NASA Langley Research Center by researchers at the University of Virginia[7,8] and the State University of New York at Buffalo.[9,10] This actuator has been extensively tested[10] and is capable of generating arbitrary control forces. The onboard microcontroller is capable of implementing colocated control laws or can serve as a local controller in a hierarchical control architecture. The actuator characteristics are described in Sec. II.

The first structure used in this study is a simple cantilevered beam constructed of a quasi-isotropic composite material being considered for use in flexible space structure construction.[11] The material has unusual damping properties[12] but is strong and lightweight. A simple experiment using the PMA and the composite beam provide a preliminary look at control/structure interaction phenomena. The actuator/composite beam system and corresponding experiment and analysis is discussed in detail in Sec. III.

The numerical study consists of using a reduced-order finite-element model of the proposed Control of Flexible Structures (COFS) I flight article.[4] The control devices mounted on the COFS I flight article are fundamentally the same as the PMA described in Sec. II. The configuration used in the study is the COFS I flight article controlled in one plane of vibration using a rate-feedback control law. This model is described in Sec. IV and analyzed for different actuator configurations in Sec. V.

II. Actuator Dynamics

The actuation device chosen for this study is the NASA/UVA/UB proof-mass actuator.[9] The actuator system is composed of a movable proof-mass, a fixed coil, two colocated sensors, a digital microcontroller, and a power amplifier as described in detail in Refs. 9 and 10. All of the actuator components are mounted as a single unit with power lines being the only external connection required by the actuator system to operate. The PMA is a reaction-type force actuator in that it creates a force by reacting against an inertial mass. Figure 1 shows an experimentally verified model of the PMA attached to a single-degree-of-freedom structural model. The dynamics of the PMA can be modeled as a single-degree-of-freedom oscillator with the addition of a force generator acting between the proof-mass and the structure. The equations of motion for this model are given as

$$\begin{bmatrix} M_s & 0 \\ 0 & m_p \end{bmatrix}\begin{bmatrix} \ddot{x}_1 \\ \ddot{x}_2 \end{bmatrix}+\begin{bmatrix} c_s+c_p & -c_p \\ -c_p & c_p \end{bmatrix}\begin{bmatrix} \dot{x}_1 \\ \dot{x}_2 \end{bmatrix} +\begin{bmatrix} K_s+k_p & -k_p \\ -k_p & k_p \end{bmatrix}\begin{bmatrix} x_1 \\ x_2 \end{bmatrix}=\begin{bmatrix} -f_g \\ f_g \end{bmatrix} \tag{1}$$

Here M_s is the equivalent lumped mass of the structure and the parasitic mass of the actuator (PMA system mass minus the proof mass). The structure is also assumed to have viscous damping coefficient C_s and stiffness K_s. The mass of the proof mass is denoted by m_p. The inherent electronic damping of the PMA system due to the back-emf in the fixed coil is denoted by c_p. The electronic stiffness force required to keep the proof mass centered in its housing is denoted by k_p. This centering force is needed in laboratory experiments to overcome the component of gravity that would cause the proof mass to slide to one end and impact the outer case. Additionally, it will be

Received March 16, 1988; revision received Sept. 21, 1988.

*Assistant Professor, Department of Aerospace Engineering, Mechanics, and Engineering Sciences, Member AIAA.

†Professor, Division of Applied Mathematics; also, Department of Mechanical and Aerospace Engineering, State University of New York, Buffalo, New York. Member AIAA.

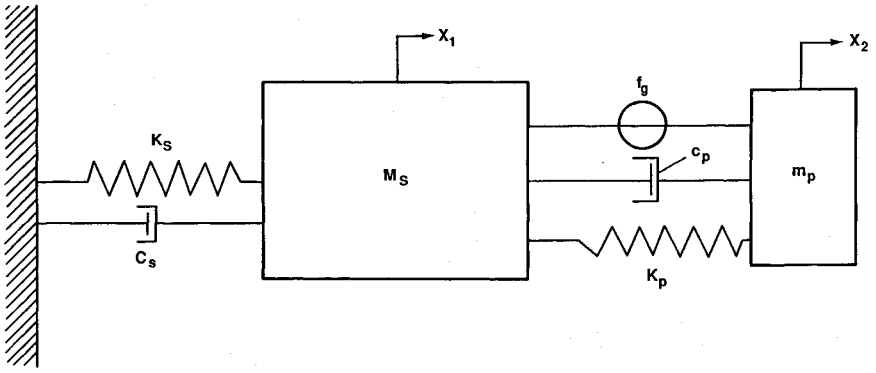

Fig. 1 Dynamic model of proof-mass actuator.

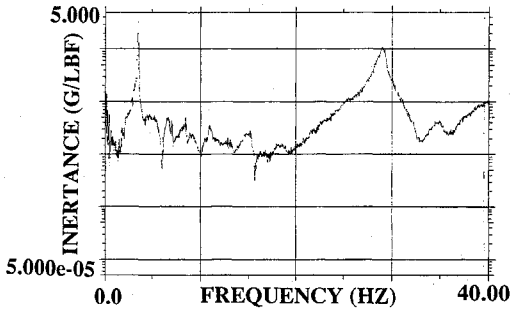

Fig. 2 Open-loop inertance frequency response function.

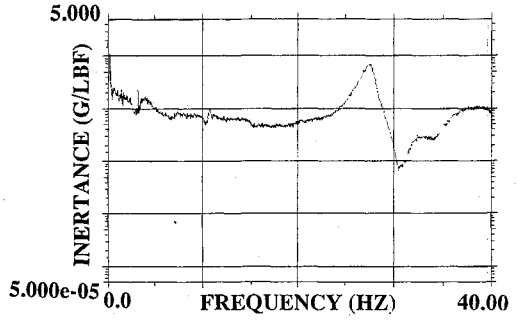

Fig. 3 Closed-loop inertance frequency response function.

shown in Sec. III that the centering force is required for the closed-loop system to be asymptotically stable. The coordinate x_1 denotes the displacement of the structure, while x_2 denotes the displacement of the proof mass. The overdots represent time derivatives. The addition of the desired control law is modeled as f_g, a force generator that applies equal but opposite forces onto the structure and the proof mass.

To determine the inherent dynamic properties of the PMA system, the actuator was attached to a nonmoving structure (M_s locked in Fig. 1). The frequency response function of the total force applied to the structure (the reactions of the spring, damper, and force generator) to the voltage command to the force generator was measured experimentally. Let $F(s)$ and $V(s)$ denote the Laplace transform of the total applied force and the voltage command to the force generator, respectively. The experimentally[9] verified transfer function for the PMA system is

$$\frac{F(s)}{V(s)} = \frac{G_1 G_2 m_p s^2}{m_p s^2 + G_1 G_2 c_p s + G_1 G_2 k_p} = G_1 G_2 \frac{s^2}{s^2 + 2\zeta_p \omega_p + \omega_p^2}$$

$$\omega_p^2 = \frac{G_1 G_2 k_p}{m_p}, \qquad 2\zeta_p \omega_p = \frac{G_1 G_2 c_p}{m_p} \tag{2}$$

Here, $G_1(N/A)$ is the electromagnetic gain of the PMA's coil, and $G_2(A/V)$ is the power amplifier gain. The inherent dynamics of the PMA are seen to be that of a high-pass filter whose characteristics are shaped by the spring and damper rates. The simplest way to characterize the dynamics of the actuator is by its break frequency ω_p, which indicates the frequency at which the Bode magnitude plot of the PMA breaks flat from a 40 dB/decade rise, and the phase plot goes through 90 deg. The break frequency corresponds roughly to the natural frequency of the actuator.

The transfer function relating the total applied force $F(s)$ and the output of the force generator $f_g(s)$ can be obtained from Eqs. (2) by considering a free-body diagram of mass m_p in Fig. 1 (again with M_s locked) and is given by

$$\frac{f_g(s)}{F(s)} = 1 - \frac{2\zeta_p \omega_p s + \omega_p^2}{s^2} \tag{3}$$

Equation (3) reveals that as $s \to \infty$, the total force applied to the structure is equal to the output of the force generator. Physically, this corresponds to the fact that both the displacement and velocity of the proof mass tend to zero as the frequency content of the force generator command signal tends to infinity.

III. Composite Beam System

An experimental test of the PMA's ability to control vibration using a rate-feedback control law was performed using a test structure made of a quasi-isotropic composite material[11] configured as a cantilevered beam. The PMA system was attached at the tip (free end). In addition to the two sensors contained within the PMA system, an independent accelerometer was mounted at the tip to monitor the vibrations of the beam. The rate-feedback control law was implemented by digitally integrating the accelerometer signal contained within the PMA system and multiplying by an appropriate gain. In this experiment, the electronic centering force gain k_p was selected such that the break frequency of the actuator was slightly lower than the fundamental mode of vibration of the cantilevered beam. A detailed description of the experimental setup, control law implementation, and experimental methods is provided in Ref. 10.

The modal properties of the uncontrolled and controlled structure were determined using both time and frequency domain identification techniques. The uncontrolled, or open-loop, system consists of the cantilevered beam with the parasitic mass of the actuator. The measured inertance (acceleration/force) frequency response function is shown in Fig. 2. Using the circle-fit identification technique,[13] the natural frequencies were determined to be 3.49 and 29 Hz, with

damping ratios of 0.2 and 1.0%, respectively. These values were also confirmed by using the eigensystem realization algorithm[14] (ERA) time domain modal identification technique.

The closed-loop system consists of the open-loop system with the proof mass added and the control law turned on. Although difficult to see from the measured inertance frequency response function of the closed-loop system in Fig. 3, an additional natural frequency appears. These three frequencies and corresponding damping ratios were again identified using the circle-fit method and verified using ERA. The closed-loop system exhibits natural frequencies at 3.19, 4.03, and 28 Hz, with damping ratios of 0.2, 9.4, and 1.9%. The appearance of a third mode of vibration is due to the PMA dynamics, and is referred to as the actuator-dominated mode. The actuator-dominated mode is the sharp narrow peak at 3.19 Hz in Fig. 3. The first structural mode is shifted up to 4.03 Hz, in accordance with the first monotonicity principle,[15] and is heavily damped by the control law.

The effect of the control system on the structure's response is best examined in the time domain. Figure 4 illustrates the open-loop time response of the accelerometer located at the tip of the beam. Examination of the response indicates that the open-loop system is very lightly damped, illustrating substantial oscillation even after 16 s have elapsed. The closed-loop system response illustrated in Fig. 5, subject to an equivalent impact, shows a substantial increase in damping, essentially reducing the structural vibration to small levels in less than 2 s. However, Fig. 5 also illustrates that a very small amplitude and lightly damped oscillation occurs at 3.19 Hz, which is the actuator-dominated mode. This oscillation represents a degradation of the closed-loop system performance because of the interaction between the structure, the control law, and the actuator dynamics.

To gain a further understanding of the structure/actuator dynamics in conjunction with the rate-feedback control law, consider a two-mode model of the controlled structure consisting of the actuator-dominated mode (3.19 Hz) and the first structural dominated mode (4.03 Hz). The second structural dominated mode (28 Hz) is not included in this model because its contribution to the total time response of Figs. 4 and 5 is minimal. The equations of motion are then given by Eq. (1), with f_g being the rate-feedback control law, $f_g = -d\dot{x}_1$. Substitution of the control law into Eq. (1) and moving the control term to the left side of the equation yields a closed-loop damping matrix of

$$\begin{bmatrix} C_s + c_p - d & -c_p \\ -c_p + d & c_p \end{bmatrix} \tag{4}$$

The homogeneous equation for the closed-loop system is no longer symmetric and positive semidefinite, indicating the possibility of an unstable response.[16] The Routh stability criteria can be utilized to determine the stable and unstable regions in the parameter space. The characteristic equation for the system is given as

$$\lambda^4 + (C_s/M_s + c_p/M_s + c_p/m_p - d/M_s)\lambda^3 + (K_s/M_s + k_p/M_s + k_p/m_p + C_s c_p/(M_s m_p))\lambda^2 + (K_s c_p/(M_s m_p) + C_s k_p/(M_s m_p))\lambda + K_s k_p/(M_s m_p) = 0 \tag{5}$$

With the aid of MACSYMA,[17] the inequality relations for the rate-feedback gain d in terms of the actuator and structural properties for a stable closed-loop system are given as

$$d < C_s + c_p + M_s c_p/m_p \tag{6a}$$

$$d < [m_p^2(K_s(C_s + c_p) + k_p(C_s + c_p) + m_p(2M_s c_p k_p + C_s c_p^2 - C_s^2 c_p) + M_s(C_s c_p^2 + M_s c_p k_p)]/[m_p^2(K_s + k_p) + m_p(M_s k_p - C_s c_p)] \tag{6b}$$

$$d \lesssim -C_s^2 c_p[1/(2K_s m_p) + 1/(2k_p m_p)] + (1/2)(C_s + c_p - K_s c_p/k_p + M_s c_p/m_p - M_s C_s k_p/K_s m_p - C_s k_p/K_s \pm \{4[(K_s(C_s m_p c_p k_p)^2 + C_s K_s^2 m_p^2 c_p^3 k_p)(M_s + m_p) + M_s C_s K_s m_p^2 c_p k_p^3(M_s + 2m_p) + K_s^3 m_p^4 c_p k_p(C_s + c_p) + C_s K_s m_p^3 c_p k_p(m_p + C_s K_s c_p) + C_s K_s m_p^3 k_p(C_s^2 k_p + C_s m_p k_p - 2M_s K_s c_p k_p)] + [(K_s m_p c_p k_p - C_s m_p k_p^2)(M_s + m_p) + C_s K_s m_p(m_p k_p - c_p^2) - c_p m_p(C_s^2 k_p + K_s^2 m_p)]^2\}^{(1/2)}/(2K_s m_p^2 k_p) \tag{6c}$$

Additionally, inspection of the last term of the characteristic equation reveals that the electronic centering force k_p is a requirement for the closed-loop system to be asymptotically stable. If no centering force is provided, the last term in Eq. (5) is zero and, thus, the system would exhibit an uncontrollable rigid-body mode. This can also be seen by examining the stiffness matrix of Eq. (1) for the case of $k_p = 0$. The existence of this rigid-body mode is independent of the choice of control law implemented by the actuator.

The physical parameters of the two-mode model described by Eq. (1) were determined by independent tests of the actuator[10] and the beam.[12,18] The constants associated with the beam dynamics M_s, C_s, and K_s were determined to be 1.1537 kg, 0.2 N-s/m, and 554.75 N/m, respectively. In determining these constants, it was assumed that the structure behaved as an ideal cantilevered beam. The constants associated with the actuator dynamics m_p and c_p (converted to mechanical units) were determined to be 0.232 kg and 0.76 N-s/m, respectively. In the control experiment, the value of k_p converted to mechanical units was 108.27 N/m. Substituting these values into Eq. (6), it is found that Eq. (6c) is the active

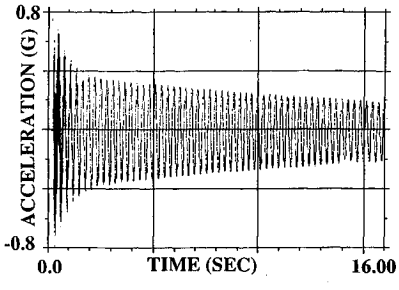

Fig. 4 Open-loop free decay tip acceleration.

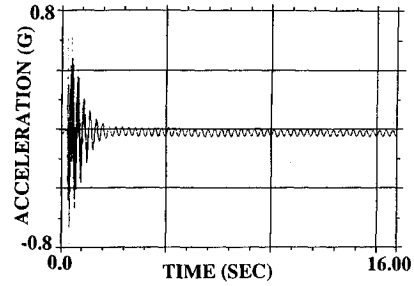

Fig. 5 Closed-loop free decay tip acceleration.

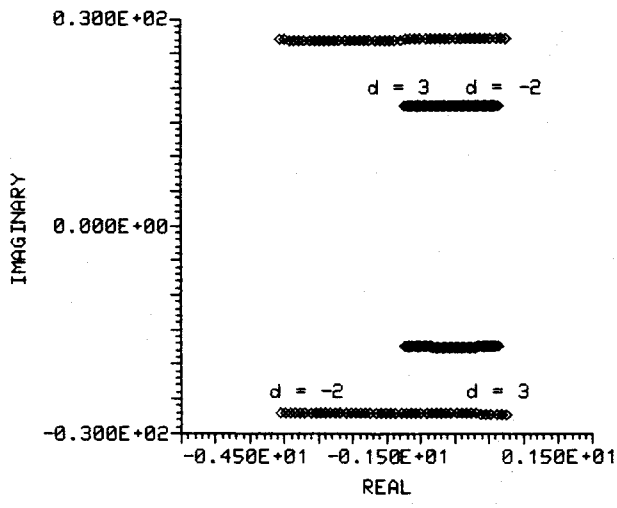

Fig. 6 System root locus.

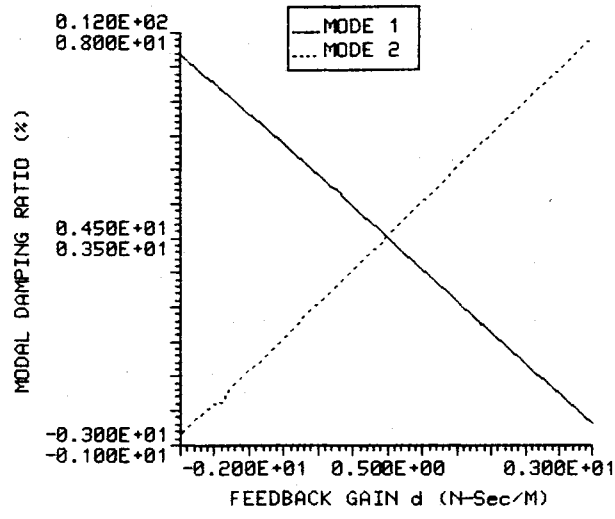

Fig. 7 Modal damping ratio vs feedback gain d.

constraint, and the rate-feedback d for a stable control system must satisfy the inequality

$$-1.55 \le d \le 2.145 \qquad \text{N-s/m} \tag{7}$$

In the active control experiment, the gain d implemented by the 8751 control program was $d = -1.2$ N-s/m, whereas the gain required to match the model damping ratios experimentally identified and those predicted by Eq. (1) is $d = -1.4$ N-s/m. This difference can be accounted for by the relative error in the identified structural parameters. In either case, the rate-feedback gain used in the experiment is relatively close to the unstable region.

The effect of the rate-feedback gain on the closed-loop poles can be demonstrated by plotting the root locus of the system transfer function. With x_1 defined to be the output and f_g the input, the root locus as a function of the rate-feedback gain d (expressed in mechanical units) is shown in Fig. 6. The root-locus plot provides information beyond that provided by Eqs. (6) for a given set of physical parameters. Specifically, Fig. 6 reveals that it is the first mode of vibration that goes unstable when the gain d is less than -1.55, and that the second mode of vibration goes unstable when the gain d exceeds 2.145. However, inspection of the root-locus plot does not directly reveal the relationship between the gain d and the modal damping ratios of the controlled structure.

A plot of the modal damping ratios vs the gain d is shown in Fig. 7. Like the root-locus plot, Fig. 7 reveals which mode goes unstable when the gain violates the Routh stability criteria. It also reveals more clearly and quantifiably that changing the gain to increase the damping in one of the modes results in a decrease in damping of the other mode. This high (in magnitude) gain instability provides an explanation of the low frequency, low amplitude, lightly damped response found in the previously described experiment, as evidenced in Fig. 5. As the magnitude of the rate-feedback gain is increased, the damping ratio of the structure-dominated mode is increased. At the same time, the damping ratio of the actuator-dominated mode decreases. Apparently the system is adding damping to one mode at the expense of the electronic damping in the actuator mode. Eventually, the gain is increased to the point where the actuator-dominated mode damping becomes negative, driving the closed-loop system unstable. The time response shown in Fig. 5 was for the closed-loop system operating at a value of gain just below that at which the system goes unstable. A classical control design would see this as a system with poor gain margin. In this region, the damping ratio is very small causing the first-mode vibration to persist for a long period of time.

IV. Structural Model

In order to investigate more thoroughly the high gain instability suggested by the simple beam experiment and analysis described in Sec. III in a large space structure application, a simplified numerical model of the COFS I truss flight article was constructed. This three-mode model consists of a two-mode approximation of the COFS I structure with an additional degree of freedom for the linear DC motor (LDCM)[4] control actuator. The three-mode model allows for an investigation into the effect of placing the break frequency of the actuator below, in between, and above the modes of vibration of the uncontrolled structure.

The LDCM developed for the COFS flight article has the same dynamic characteristics as the PMA discussed in Sec. II.[4] Therefore, Eq. (2) is also the transfer function for the LDCM control actuators. A continuum beam model[4] of the truss developed for control law design studies was used. The equivalent beam characteristics are given as length 60.693 m, mass per unit length 4.461 kg/m, and flexural rigidity 28.63×10^6 N-m^2. The continuum model was then approximated using a statically reduced two-element finite-element model. Nodes zero, one, and two were located at the base, mid-point, and tip of the beam, respectively, as shown in Fig. 8. This physical modeling approach was used as an alternate approach to the more standard modal model because the interaction of the actuator and structural dynamics become more apparent. A lumped mass (100 kg) was added at the tip of the beam. The open-loop natural frequencies for this approximate model are calculated to be 1.429 and 10.39 rad/s. The equations of motion of the controlled system are given as

$$\begin{bmatrix} 140.8 & 0 & 0 \\ 0 & 170.4 & 0 \\ 0 & 0 & m_p \end{bmatrix} \begin{bmatrix} \ddot{x}_1 \\ \ddot{x}_2 \\ \ddot{x}_3 \end{bmatrix} + \begin{bmatrix} 0 & 0 & 0 \\ 0 & c_p & -c_p \\ 0 & -c_p & c_p \end{bmatrix} \begin{bmatrix} \dot{x}_1 \\ \dot{x}_2 \\ \dot{x}_3 \end{bmatrix}$$

$$+ \begin{bmatrix} 14045 & -4395 & 0 \\ -4395 & 1752 + k_p & -k_p \\ 0 & -k_p & k_p \end{bmatrix} \begin{bmatrix} x_1 \\ x_2 \\ x_3 \end{bmatrix} = \begin{bmatrix} 0 \\ f_g \\ -f_g \end{bmatrix} \tag{8}$$

where x_1 and x_2 are the displacements of the two finite-element model nodes of the truss at the midpoint and tip, and x_3 is the displacement of the proof mass.

V. Actuator Limitation

In this section several cases of actuator design are considered to point out control system design limitations and to investigate the nature of the interaction between the control

law, the actuator dynamics, and the structural dynamics. The criteria used to explain the nature of this interaction is to examine the modal damping ratios of the closed-loop system as a function of the rate-feedback gain d.

First, consider the common case of control system design without considering the actuator dynamics. Figure 9 illustrates that increasing the control gain d substantially increases the damping ratio of mode 1. In addition, the second-mode damping ratio is also increased, but to a much lesser extent, due to placement of the control actuator near the node of the second mode. This naive modeling approach seems to indicate that a reasonable design exists for reducing vibration levels in the first mode. The danger of this modeling approach is illustrated in the following.

Next, consider the addition of the actuator dynamics to the previous case. The break frequency ω_p is chosen to be less than the first structural mode [$\omega_p = 0.5 < 1.43 = \omega_1$ (rad/s)]. In this case the closed-loop equations become

$$\begin{bmatrix} 140.8 & 0 & 0 \\ 0 & 170.4 & 0 \\ 0 & 0 & 22 \end{bmatrix} \begin{bmatrix} \ddot{x}_1 \\ \ddot{x}_2 \\ \ddot{x}_3 \end{bmatrix} + \begin{bmatrix} 0 & 0 & 0 \\ 0 & 1.1+d & -1.1 \\ 0 & -1.1-d & 1.1 \end{bmatrix} \begin{bmatrix} \dot{x}_1 \\ \dot{x}_2 \\ \dot{x}_3 \end{bmatrix}$$

$$+ \begin{bmatrix} 14045 & -4395 & 0 \\ -4395 & 1757.5 & -5.5 \\ 0 & -5.5 & 5.5 \end{bmatrix} \begin{bmatrix} x_1 \\ x_2 \\ x_3 \end{bmatrix} = \begin{bmatrix} 0 \\ 0 \\ 0 \end{bmatrix} \qquad (9)$$

where $c_p = 1.1$ (N-s/m) results from assuming that the actuator back-emf damping is 5%. The mass m_p used in Eq. (9) is consistent with the moving mass of the pair of LDCM tip actuators mounted in one plane on the COFS flight hardware. The 5% modal damping ratio of the inherent actuator dynamics is representative of measurements of various PMA's built.

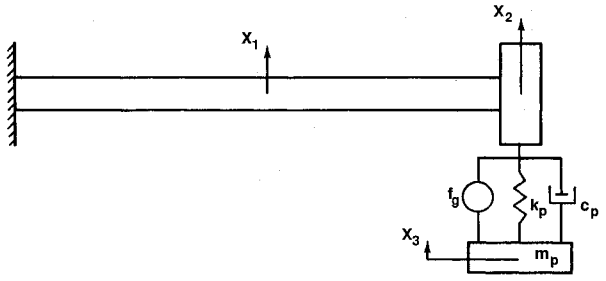

Fig. 8 Equivalent continuum beam and actuator configuration.

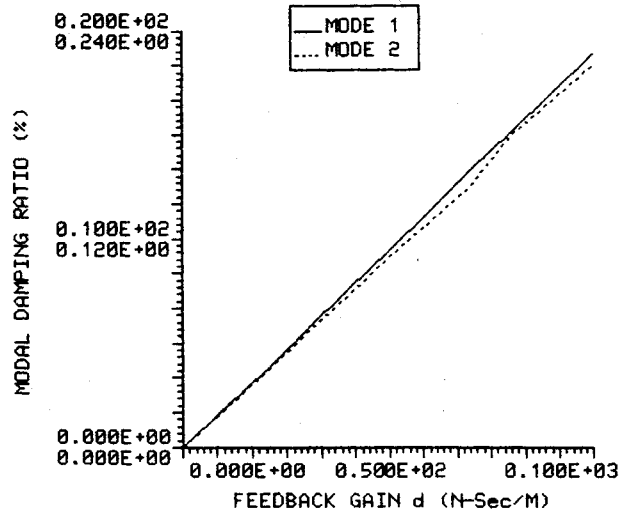

Fig. 9 Damping vs gain—actuator dynamics ignored.

The undamped ($c_p = d = 0$) eigenvalues and eigenvectors are

$$\omega_1 = 0.496 \text{ rad/s}, \quad \underline{u}_1 = [0.0051 \quad 0.163 \quad 1.0]^T$$

$$\omega_2 = 1.44 \text{ rad/s}, \quad \underline{u}_2 = [0.3196 \quad -1.0 \quad -0.1369]^T$$

$$\omega_3 = 10.39 \text{ rad/s}, \quad \underline{u}_3 = [1.0 \quad -0.2640 \quad 0.006]^T \qquad (10)$$

The first mode of vibration is termed actuator-dominated because the third coordinate, which corresponds to the actuator displacement, illustrated the largest amplitude, whereas the other two coordinates are relatively small. By this criteria, modes 2 and 3 are structure-dominated, but both have some actuator influence.

The modal damping ratios for this case are plotted vs the gain in Fig. 10. Note that, again, the first structure-dominated mode (mode 2) shows an increase in damping ratio, from almost zero for the open-loop system, to as much as 20% for the high-gain closed-loop case. Again, the other structure-dominated mode increases in damping as well. However, note that the damping ratio of the actuator-dominated mode (mode 1) decreases with increasing gain. In fact, there is some value of the gain at which the modal damping ratio becomes negative, driving the closed-loop system unstable. This again represents a high-gain limitation on the local rate-feedback control law, the actuator, and the structure.

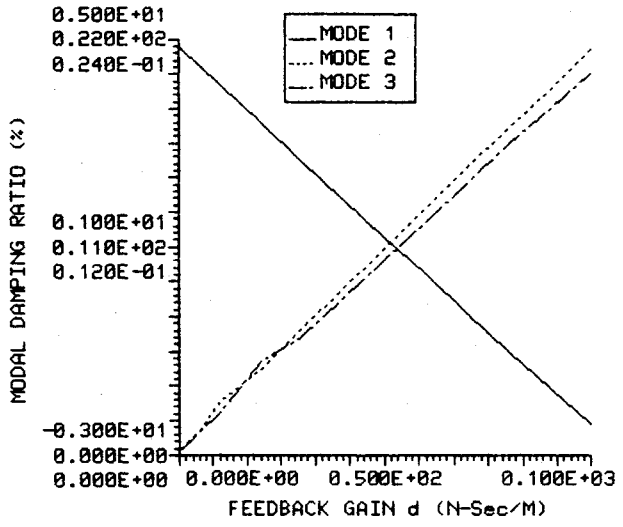

Fig. 10 Damping vs gain, $\omega_p < \omega_1$.

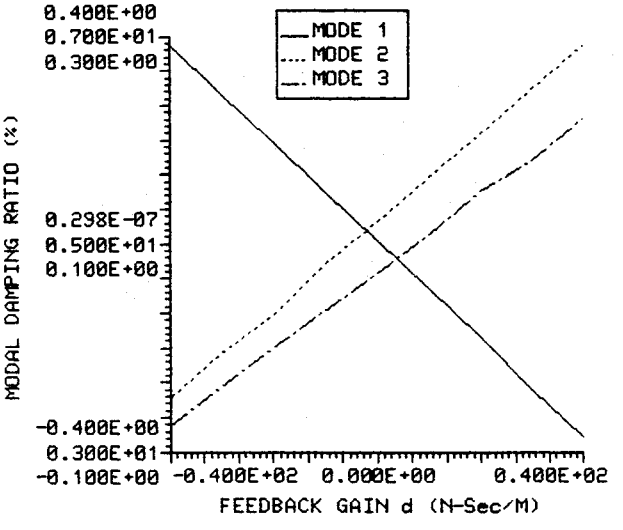

Fig. 11 Damping vs gain, $\omega_1 < \omega_p < \omega_2$.

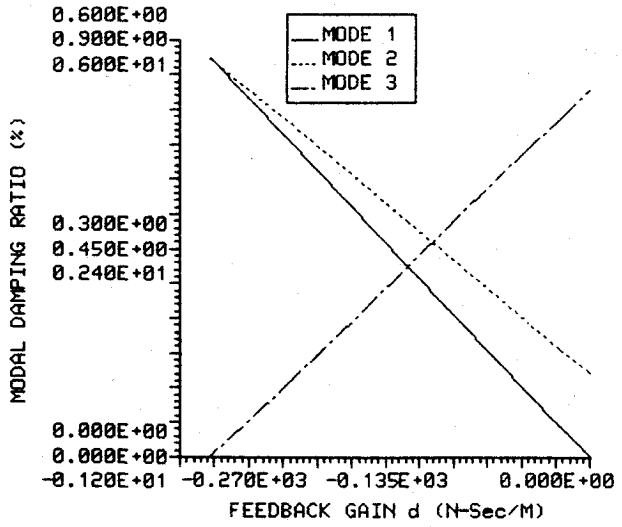

Fig. 12 Damping vs gain, $\omega_p > \omega_2$.

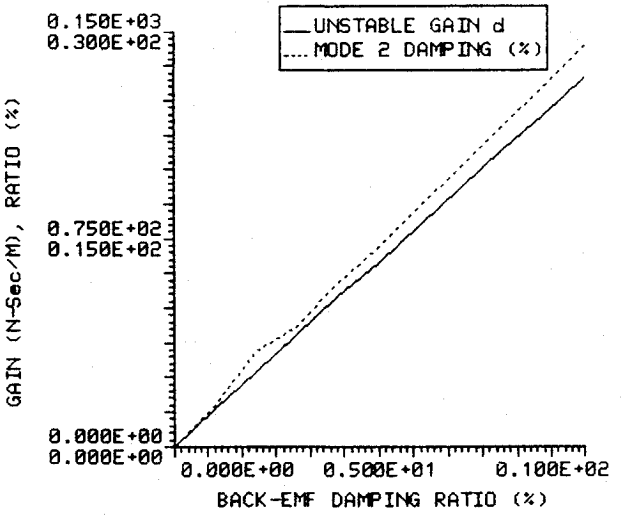

Fig. 13 Modal stability design chart.

Next, consider the case that the break frequency is chosen to fall in between the two structural frequencies. Specifically, consider $\omega_1 = 1.35 < \omega_p = 6 < \omega_2 = 10.41$. An eigenvector analysis of this system reveals that mode 1 is dominated by both the structure and the actuator, mode 2 is actuator dominated, and mode 3 is structure dominated. The modal damping ratios of each mode are plotted vs the actuator gain in Fig. 11. Note that in this case, one of the damping ratios is negative for almost any nonzero value of the gain that achieves reasonable structural damping. Hence, the closed-loop system is almost always unstable, and selecting the break frequency of the actuator to lie between two structural modes is not feasible (without further compensation). This is due to the phase characteristics of the PMA. For the rate-feedback control law, the voltage command to and force output of the force generator will have a frequency content equal to the damped natural frequencies of the closed-loop system. For a stable closed-loop system, the sign of the rate-feedback gain is chosen such that the force component at each individual frequency opposes the corresponding modal velocity of the structure. At frequencies well below the break frequency of the actuator, there is an 180-deg phase difference between the voltage command and the actual applied force, whereas at frequencies well above the break frequency, there is no phase difference. Therefore, when the break frequency of the actuator is chosen to lie in between two of the structural modes and the voltage command corresponds to a physical velocity (not a known sum of individual modal velocities), the individual applied force components on one side of the break frequency will oppose the corresponding modal velocities, thereby removing energy from these modes. However, because of the 180-deg phase difference, the individual applied force components on the other side of the break frequency will aid the modal velocities, thereby adding energy to these modes. If the energy dissipated by the inherent modal damping of these modes is not greater than the energy added by the applied force components, the closed-loop system will become unstable.

Some researchers[19] have suggested that placing the break frequency of the actuator above the highest frequency of interest is a feasible method of reducing the effects of actuator dynamics on control design. Several problems arise in the control structure configuration examined here. First, because the magnitude of the actuator force output breaks down at 40 dB/s below the break frequency, the output force level would be severely limited at low frequencies, typically where the highest levels of control force are required. Secondly, if the structure is very flexible, the model approaches a partial differential equation model with an infinite number of frequencies, as pointed out in Ref. 20. Hence, there is always some structural frequency larger than the break frequency, and the unstable closed-loop situation of Fig. 11 results. In addition, the high-gain instability problem of the previous case is still present. In practical terms, although a structure does not exhibit the infinite number of frequencies the partial differential equation would predict, the question of how one would pick the highest structural frequency that can be excited is not yet answered.

With $\omega_p > \omega_2$, eigenvector analysis reveals that the actuator effect is strongly present in each mode with the third mode being clearly actuator dominated. Figure 12 illustrates the modal damping ratio vs gain plots for each of the modes. Note that increasing the feedback gain increases the modal damping, but to a much smaller extent than for the case with the break frequency below the first structural frequency indicated in Fig. 10. In fact, for the case considered, the highest achievable closed-loop damping ratio is less than 1%. This happens because the actuator is force-output limited in this condition, as described in the previous paragraph. Again, the system goes unstable at higher values of the gain. At least for the system configuration presented here, placing the actuator break frequency above the highest structural frequency offers no apparent advantage.

Returning to the case with the break frequency chosen to be smaller than the lowest structural natural frequency, the high-gain limitation can be represented in terms of the modal design chart of Fig. 13. This is also used to illustrate the importance of back-emf damping in actuator design. The solid line of Fig. 13 divides the plot into stable and unstable regions. For a given back-emf actuator damping ratio (defined by ζ_p), the solid line yields the largest feedback gain before the system becomes unstable. This curve represents the systems' high-gain limit. The dashed line indicates the maximum achievable damping ratio for the second mode (which is the first structural mode) before the high-gain instability occurs.

VI. Summary

The interaction between a structure, an actuator used to control the structure, and the control law used to drive the system has been examined for two different systems. The first system considered consisted of a simple cantilevered beam controlled using a rate-feedback control law implemented by a proof-mass actuator. The second system consisted of controlling the vibrations of the COFS I flight article using a rate-feedback control law implemented by a Linear DC

Motor. A simplified model of the COFS I structure was used so that the control/structure interaction phenomena were more clearly revealed. In the past, the simple rate-feedback control law has been viewed as being a stable control law, because it is equivalent to an increase in the passive damping level of the structure. However, when proof-mass actuator dynamics are included, it was shown that a high-gain instability prevents arbitrarily high levels of damping from being added to the system by active control. This high-gain instability was investigated using Rouths' stability criteria in a general sense and through root-locus and modal damping plots for specific cases.

With added damping to the first (lowest) structural mode as a design criteria, it was shown that the break frequency of the actuator should be designed below the first natural frequency of the structure for best performance. In addition, it was shown that the closed-loop system exhibits a high-gain limitation, and that this limitation is determined by the amount of back-emf damping available. It was also shown that as the high-gain limit of a given structure/actuator/control law configuration is approached, system performance degrades substantially.

Acknowledgments

This work was supported in part by NASA Grants NGT 33183801 and NAG-1985 through the Structural Dynamic Branch of NASA Langley Research Center, Air Force Office of Scientific Research Grants 85-0220 and F49620-86-6-0111 through the Mathematics and Information Sciences Directory, and National Science Foundation Grant MSM 8351807. The instrumentation was provided by Equipment Grant AFOSR 850119. The composite beam and the proof-mass actuator were provided by the Structural Dynamics Branch of NASA Langley Research Center through the efforts of R. Miserentino and G. C. Horner.

References

[1]Juang, J.-H. and Longman, R. W. (eds.), "Special Issue on Structural Modeling and System Identification of Flexible Space Structures," *Journal of the Astronautical Sciences*, Vol. 33, No. 1, Jan.-March, 1985.

[2]Meirovitch, L. (ed.), *Proceedings of the Sixth VPI&SU/AIAA Symposium on the Dynamics and Control of Large Structures,* Virginia Polytechnic Inst. and State Univ., Blacksburg, VA, June-July 1987; also see proceedings of preceding years, 1977, 1979, 1981, 1985.

[3]Balas, M. J., "Trends in Large Space Structure Control Theory: Fondest Hopes, Wildest Dreams," *IEEE Transactions on Automatic Controls*, Vol. AC-27, No. 3, June 1982, pp. 522–535.

[4]Wright, R. L. (ed.), *Proceedings of the 1st NASA/DOD Control/Structures Interaction Technology Conference*, Norfolk, VA, NASA CP-2447, Pts. 1 and 2, Nov. 1986.

[5]Swanson, A. D. (ed.), NASA/DOD Control/Structures Interaction Technology—1987, Colorado Springs, CO, AFWAL-TR-88-3052, Nov. 1987.

[6]Caughey, T. K. and Goh, C. J., "Vibration Suppression in Large Space Structures," *Proceedings of the Workshop on Applications of Distributed System Theory to the Control of Large Space Structures*, Jet Propulsion Lab., Pasadena, CA, Pub. 83–46, 1983, pp. 119–142.

[7]Pilkey, W. D. and Haviland, J. K., "Large Space Structure Damping Design—Final Report," Univ. of Virginia, Charlottesville, VA, 1983.

[8]Haviland, J. K., Lim, T. M., Pilkey, W. D., and Politansky, H., "The Control of Linear Dampers for Large Space Structures," *Proceedings of the 1987 AIAA Guidance and Control Conference*, AIAA, New York, Aug. 1987, pp. 106–116.

[9]Zimmerman, D. C., "Dynamic Characterization and Microprocessor Control of the NASA/UVA Proof-Mass Actuator," M.S. Thesis, Dept. of Mechanical and Aerospace Engineering, State Univ. of New York at Buffalo, Buffalo, NY, June 1984.

[10]Zimmerman, D. C., Horner, G. C., and Inman, D. J., "Microprocessor Controlled Force Actuator," *Journal of Guidance, Control, and Dynamics,* Vol. 11, No. 3, May–June 1988, pp. 230–236.

[11]Wilson, M. L. and Miserertino, R., "Pertrusion Process Development for Long Space Boom Models," *Proceedings of the 41st Annual Conference of the Society of Plastics Industry*, institute paper 60, Jan. 1986.

[12]Banks, H. T., Cudney, H. H., Inman, D. J., and Wang, Y., "Parameter Identification Techniques for the Estimation of Damping in Flexible Structure Experiments," *Proceedings of the 26th IEEE Conference on Decision and Control*, Research Studies Press, Letchworth, England, UK, Dec. 1987.

[13]Ewins, D. J., *Modal Testing: Theory and Experiment*, Research Studies Press, 1986.

[14]Juang, J.-N. and Pappa, R. S., "An Eigensystem Realization Algorithm for Modal Parameter Identification and Model Reduction," *Journal of Guidance, Control, and Dynamics*, Vol. 8, Sept.-Oct. 1984, pp. 620–627.

[15]Weinberger, H. F., "Variational Methods for Eigenvalue Approximation," *Regional Conference Series in Applied Mathematics*, Society of Industrial and Applied Mechanics, Philadelphia, PA, March 1974, pp. 58–62.

[16]Inman, D. J., "Dynamics of Asymmetric Nonconservative Systems," *Journal of Applied Mechanics*, Vol. 50, No. 1, 1983, pp. 199–203.

[17]Bogen, R., *MACSYMA Reference Manual*, Version 10, Mathlab Group, Massachusetts Inst. of Technology, Cambridge, MA, 1983.

[18]Zimmerman, D. C. and Cudney, H. H., "Practical Implementation Issues for Active Control of Large Flexible Structures," *ASME Journal of Vibration, Acoustics, Stress, and Reliability in Design*, Vol. 111, No. 3, July 1989, pp. 283–289.

[19]Balas, M. J., "Observer Stabilization of Singularly Perturbed Systems," *Journal of Guidance and Control*, Vol. 1, Jan.–Feb. 1978, pp. 93–95.

[20]Goh, C. J. and Caughey, T. K., "On the Stability Problem Caused by Finite Actuator Dynamics in the Colocated Control of Large Space Structures," *International Journal of Control*, Vol. 41, No. 3, March 1985, pp. 787–802.